Doping-induced dimensional crossover and thermopower burst in Nb-doped $SrTiO_3$ superlattices

P. Delugas,[1] A. Filippetti,[1] M. J. Verstraete,[2] I. Pallecchi,[3] D. Marré,[3] and V. Fiorentini[4]

[1] *CNR-IOM, UOS Cagliari, S.P. Monserrato-Sestu Km. 0.700, Monserrato (CA), Italy*
[2] *Département de Physique, B5a, Université de Liège, B-4000 Sart-Tilman, Belgium*
[3] *CNR-SPIN UOS Genova and Dipartimento di Fisica, Via Dodecaneso 33, 16146 Genova, Italy*
[4] *CNR-IOM, UOS Cagliari and Dipartimento di Fisica, Università di Cagliari, Monserrato (CA), Italy*

(Dated: May 22, 2013)

Using advanced ab-initio calculations, we describe the formation and confinement of a two-dimensional electron gas in short-period (≃4 nm) Nb-doped $SrTiO_3$ superlattices as function of Nb doping. We predict complete two-dimensional confinement for doping concentration higher than 70%. In agreement with previous observations, we find large thermopower enhancement at room temperature. However this effect is primarely determined by the charge dilution over a multitude of weakly occupied bands. As a general rule, we conclude that thermopower in heterostructures is more enhanced by weak, rather than tight, spatial confinement.

PACS numbers: 73.20.At, 73.40.Lq, 73.50.Lw, 73.63.Hs

I. INTRODUCTION

Since the discovery of 2-dimensional (2D) electron gas (2DEG) in $SrTiO_3/LaAlO_3$[1], the search of oxide heterostructures with charge-confinement characteristics has been relentlessly pursued by the solid state community. Among the many qualities attributed to 2DEGs, one of the most appealing is the large thermoelectric power. There is mounting evidence, indeed, that nanostructured systems[2–7], rather than bulk materials, can provide a new generation of highly efficient thermoelectric devices capable to directly convert temperature (T) gradients into electric power, and viceversa, thus providing efficient heating and cooling functionalities[8].

Recently, large thermopower was observed in several delta-doped $SrTiO_3$ (STO) superlattices[9,10]. In the 20% Nb-doped $SrTiO_3$ (STO) superlattices (SLs)[9,12,13], alternating n layers of insulating STO with m layers of 20% Nb-doped STO (STO_n/Nb-STO_m) the measured in-plane thermoelectric power, or Seebeck coefficient S, is several times larger than in STO bulk at the same doping. This was hypothesized as due to a density of states (DOS) increase induced by 2D localization[14–17]. However, this scenario remains to be proved since, in absence of a microscopic description of the system, the presence of a 2D-confined electron gas cannot be assessed. Furthermore, the multi-band nature of transport in oxide heterostructures may give rise to quite a complicated thermoelectric behavior (as seen e.g. for $SrTiO_3/LaAlO_3$[18]) whose understanding requires the detailed microscopic description of the heterostructure.

In this Letter we describe the 10-layer STO_9/Nb-STO_1 SL, formed by the alternance of one Nb-doped layer and a barrier of 9 undoped STO layers at varying Nb-doping concentration. This SL was first considered in Ref.9, while later works by the same authors[12,13] extended the study to SLs with a varying number of layers, but always keeping 20% Nb-doping. Here we study fully from First-Principles three Nb-doping concentrations (25%, 50%, and 100% doping) which are all relevant for experiments since pulsed laser deposition of Nb-doped STO is achievable in the whole 0-100% doping range[11]. Our study is then extended to generic Nb-doping concentration by the use of a multiband effective mass model.

We show that the Nb concentration directly controls the properties of the electron gas. In particular, for large enough nominal doping, a fully confined 2DEG is formed in this short (10-layer period) SL. Furthermore, in agreement with experiment, the Seebeck in the SL is larger than in STO bulk at the same nominal doping. Our space-resolved analysis of thermopower shows that the major increase in thermopower should be lead back to the redistribution of mobile charge in the many bands accessible at finite temperature, i.e. to the charge dilution across a region of several nm size thickness. This result agree with the arguments of Ref.10, where the observed large thermopower for La-doped STO SL was related to the spilling of charge carriers out of the doped region. Our results indicate that, as a general rule, in multiband systems weak 2D confinement is more favorable to large thermopower than strong 2D confinement.

II. METHODS: BEYOND-LDA BAND STRUCTURES COMBINED WITH BLOCH-BOLTZMANN APPROACH

To describe the SL we use the ab initio variational self-interaction-corrected density-functional approach (VPSIC)[19], successfully applied to many oxides including STO/LAO[18,20] and LNO/LAO[21] superlattices. Such an advanced approach is essential because the band gap error in standard local density functionals may affects band positions and alignments, thus severely compromising the accuracy of SL transport properties. For the SL we describe doping by actual atomic substitutions and explicitly recalculate all properties (including

atomic relaxations and electronic structure) at each doping, which is mandatory because the rigid band approximation tipically fail in oxide heterostructures. For the bulk, full atomic relaxations are performed at 25% doping, while values at different dopings are obtained using rigid band approximation, which works well for bulk.

For the determination of the Seebeck (S) coefficient in diffusive regime, we employ the well known Bloch-Boltzmann transport equations solved in relaxation time approximation (BBT), as implemented in the BotzTraP code[22]. The BBT requires two main ingredients as an input: the electronic band structure and the relaxation time τ. The band structures are calculated by VPSIC on very dense k-space grids (30×30×30 corresponding to 680 k-points in the IBZ for STO bulk, and 20×20×3 giving 230 k-points in the IBZ for the SLs) and interpolated by the linear-tetrahedron approach. The relaxation time τ tipically depends on carrier energy ϵ and temperature, and is overwhelmingly difficult to be calculated ab-initio for a generic scattering regime, so that it is often assumed to be constant. Within constant relaxation time (CRT) the calculation is quite simplified since τ cancels out of the expression of Seebeck and Hall resistivity, thus making these two quantities parameter-free and fully determined by the band structure alone. As a further bonus, for τ ∼const the Hall factor r_H is equal to unity, Hall and conduction mobility ($\mu_H = \mu\ r_H$) become identical, and the Hall resistivity (R_H=r_H/(n_{3D}e)) is simply the inverse of the 3D charge density.

While very computationally favourable, it will be shown in the next Section that CRT is rather unsatisfying for what concern the quantitative agreement with the measurements. Then, looking for a route towards an analytical determination of τ which could a) overcome the gross disagreement with the experiment, b) depend on the lowest possible number of parameters and simple enough to keep calculations feasible even for large-size systems such as oxide heterostructures, we adopt for τ a simple ansatz suggested in literature[24,25], based on the factorization in temperature-dependent and energy-dependent parts:

$$\tau(\epsilon, T) = F(T) \left(\frac{\epsilon - \epsilon_0}{K_B T} \right)^{\lambda}, \qquad (1)$$

where ϵ_0 is the conduction band bottom, λ a phenomenological parameter, and F(T) an energy-independent prefactor. The unknown prefactor F(T) cancels out in the expression of Seebeck and Hall resistivity, thus we are left with λ as the only parameter. Herafter we will fix λ=3/2 which optimally reproduces the Seebeck measurement in the whole temperature range (this was previously noticed in Ref.24 where Eq.1 is used in combination with an effective-mass model expression of S). A possible ambiguity of this choice resides in the fact that $\epsilon^{3/2}$ is the leading term (for the low-doping regime) of the Brooks-Herring (BH) expression of τ for ionized-impurity scattering, which is hardly dominant in STO above temperature of 100 K, where a predominance of polar-optical phonon scattering should be expected. However, notice that Eq.1 is radically different from the BH formula (which has a more complicated T-depencence through the Debye screening length and cannot be reduced to the form given in Eq.1). In other words, λ in Eq.1 must be interpreted as a phenomenological fitting parameter, and its effect on the calculated $S(T)$ not related to the predominance of the impurity scattering regime as described by BH.

Adopting Eq.1 the BBT calculation thus remains at the same level of a mere CRT approximation. And yet, it will be showed that use of Eq.1 is capable to greatly improve the CRT results for STO-based systems (and probably for wide-gap oxides in general).

III. STO BULK

To validate our methodology, we first consider the transport properties of doped bulk $SrTiO_3$ (STO), that are well described in a number of experiments. For thermopower measurements, we compare our results to two detailed works: Ref.24 for low-T data (below 300 K), and Ref.26 for high-T data (up to 1200 K). Our BBT results for S(T) obtained using Eq.1 with λ=3/2 and λ=0 (CRT approximation) are shown in Fig.1 for selected doping values matching those reported in the abovementioned references (Fig.2 of Ref.24 and Fig.1 of Ref.26).

The comparison clearly demonstrates that our analytic modeling produces a dramatic improvement over the CRT approximation. In the latter, S appears visibly underestimated in absolute value, and its temperature-dependence rather shapeless, with respect to the measurements. On the other hand, the adoption of energy-dependent τ restores a good qualitative agreement with the experiment for a wide range of doping values. Even quantitatively the match with the experiments is rather satisfying, also considering the uncertainty in the actual carrier concentration reported in the experiment (an evidence of this aspect is given later on with the analysis of Hall resistivity). An exception to this good match is the negative phonon-drag peak at T=50 K measured for the least doped sample of Ref.24 (see Fig.2 of Ref.24); in fact, phonon-drag is not implemented in our BBT calculation which at present only includes the diffusive term. It is remarkable, in particular that the same value of λ can interpolate two sets of measurements obtained in distinct experiments for a very different range of temperatures. This testifies the good universality of the model, at least for what concerns wide-gap insulating oxides.

An important quality check for Eq.1 can be obtained from Hall resistivity calculation, which, like S, does not depend on prefactor F(T) and then it can be calculated plugging the energy-dependent part of Eq.1 into the BBT. In Refs.24 and 26 R_H measurements are not reported, thus we compare calculations with our own Hall measurement for two STO bulk samples (previously used in Ref.18) corresponding to two different ranges of doping

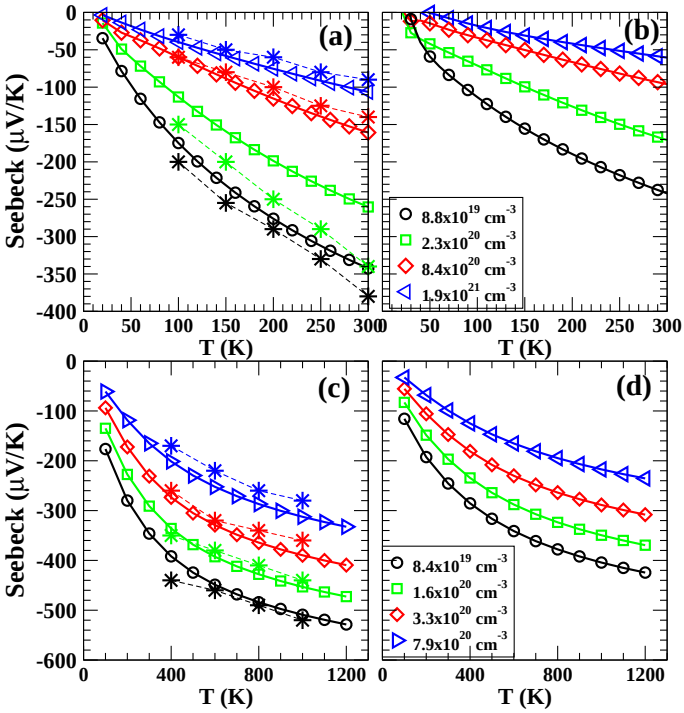

FIG. 1: Seebeck calculated by BBT approach for STO bulk. Left panels: calculations for τ given in Eq.1 with λ=3/2; right panels: calculation with λ=0 (i.e. constant τ). Top-panels refers to doping concentrations reported in Ref.24, bottom panels to the concentrations reported in Ref.26. To facilitate the comparison with these experiments, a crude hand-made extrapolation for some experimental data (star symbols) is also included.

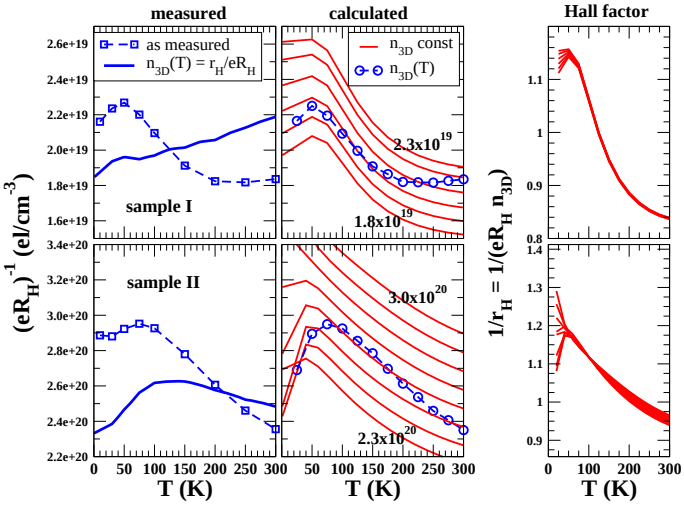

FIG. 2: Left panels: measured inverse Hall resistivity $(eR_H)^{-1}$ for two STO bulk samples, a lightly-doped sample I (top) and a heavily-doped sample II (bottom panel). Blue squared symbols show $(eR_H)^{-1}$ as measured, blue solid line the carrier density $n_{3D}(T)=r_H/(eR_H)$ obtained rescaling the measured Hall resistivity by the calculated Hall factor r_H. Central panels, red lines: $(eR_H)^{-1}$ calculated for a range of fixed densities spanning the experimental doping range: from 1.8×10^{19} cm^{-3} to 2.3×10^{19} cm^{-3} with incremental steps of 0.1×10^{19} for sample I (top); from 2.3×10^{20} cm^{-3} to 3.0×10^{20} cm^{-3} with increments of 0.1×10^{20} for sample II (bottom). Central panels, blue circlets: $(eR_H)^{-1}$ calculated for the variable charge density $n_{3D}(T)$ given by the solid line in the left panel, to be directly compared with the measured vaues (blue squares) to the left. Right panels: Hall factors $r_H=(eR_H)n_{3D}$ obtained rescaling eR_H calculated at fixed n_{3D} (red curves of central panels) with these densities. Clearly r_H is weakly dependent on n_{3D}, but strongly T-dependent. The average r_H over these densities is used to rescale the measured Hall resistivity and determines $n_{3D}(T)$ in the left panels.

concentration. The match between calculated and measured S for these samples was already shown in Ref.18 to be excellent, thus we can focus just on R_H. In Fig.2 (left panels) we report $(e\,R_H)^{-1}$ measured for the two samples below T=300 K, to be compared with the calculated values (central panels). The shape of calculated and measured values are nicely similar for both samples, however a direct quantitative comparison is complicated since $(e\,R_H)^{-1}$ obviously depends on the carrier concentration n_{3D}, which in the calculation is constant with T and known by construction, while in the experiment is unknown and tipically varying with T. To circumvent this ambiguity, we proceeded as following: i) $(e\,R_H)^{-1}$ is calculated (red lines of central panels) for a range of fixed doping values spanning the experimental range of $(e\,R_H)^{-1}$ (for the first sample from 1.8×10^{19} cm^{-3} to 2.3×10^{19} cm^{-3}, for the second samples from 2.3×10^{20} cm^{-3} to 3.0×10^{20} cm^{-3}). ii) From each of these curve we can easily evaluate the Hall factor as $r_H = (e\,R_H\,n_{3D})$ (red curves in the right panels). According to the effective-mass models, we expect r_H to depend only on λ, and be equal to unity for λ=0. Indeed, our calculated r_H is almost independent on the density (except at low temperature), and very different from unity, as expected having used λ=3/2. iii) the r_H average over the considered range of densities is calculated, and then used to rescale the measured $(e\,R_H)^{-1}$ and obtain an estimate of the true carrier concentration as a function of T for the two considered samples (left panels, blue lines). iv) Finally, we can use this estimate of $n_{3D}(T)$ to recalculate $(e\,R_H)^{-1}$ at varying charge density, thus now directly comparable with the experiment (squared symbols in central panel).

We can appreciate the excellent quantitative agreement of calculated and measured Hall resistivity for both samples in the whole temperature range, apart for T lower than 25 K (at low temperature the BBT numerical integration requires extremely dense k-point grids, thus numerical accuracy is very difficult to achieve). We emphasize that it is customary in literature to discard the Hall factor and present the measured $(eR_H)^{-1}$ (with its oscillating behaviour as a function of T) as the Hall-measured charge carrier density, for which oscillations do not make much sense. Once renormalized by the Hall factor, the estimated carrier density display a more plausible

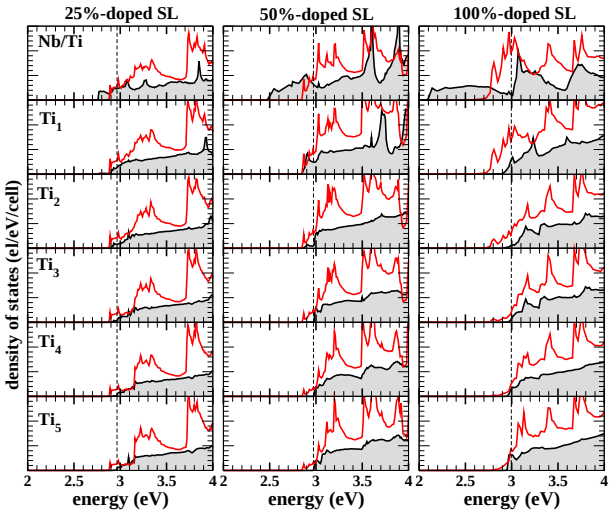

FIG. 3: Nb- and Ti-projected DOS of conduction t_{2g} states in the STO_9/Nb-STO_1 superlattice at 25%, 50%, and 100% Nb concentration (gray shaded lines: d_{xy}; red lines: d_{xz}+d_{yz}). Top panel is the doped layer, lowest panel the STO layer furthest from the doped side. Dashed lines: Fermi energy (energy zero: valence band top).

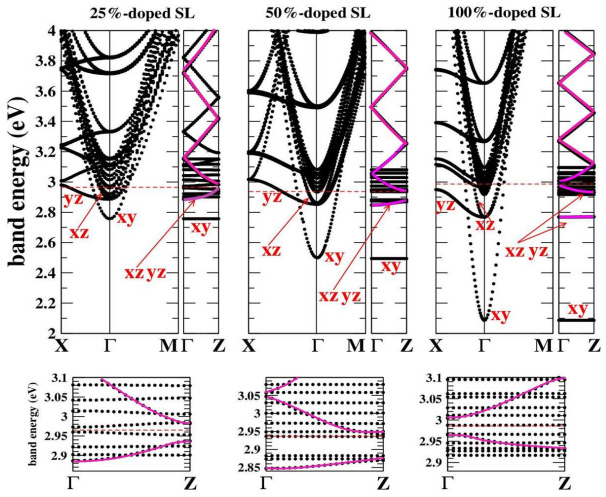

FIG. 4: Top: bands of the STO_9/Nb-STO_1 SL at 25%, 50%, and 100% doping. Dashed lines are Fermi energies; energy zero is placed at the valence band top. The character of the three lowest bands is labeled. The conduction bands of d_{xz}, d_{yx} character along Γ-Z=[001] are highlighted in violet: with increasing Nb doping, a gap opens between the flat lowest branch and the higher downfolded bulk-like sections. Bottom: enlargement of the bands around ϵ_F.

thermally-activated increase with temperature.

In conclusion, our calculation for Seebeck, Hall resistivity and Hall factors based on Eq.1 show a nice quantitative agreement with the experiments and a dramatic improvement over CRT results at null increase of computing cost. This validate the application of the method to the Nb-doped STO SLs, presented in the following.

IV. STO SUPERLATTICE

A. Electronic properties

The DOS of STO_9/Nb-STO_1 SL at 25%, 50%, and 100% Nb doping is reported in Fig.3. At 100% doping, the Ti-substituting Nb donates one electron per unit cell area to the SL conduction bands, but the strongly electronegative Nb^{1+} ion keeps most of the mobile charge to itself. As evident from the Figure, at 100% doping a large portion (0.75 electrons) of this charge remains in the 3d orbitals of the doped layer, 40% of which in the planar d_{xy} and 30% in each of the d_{xz} and d_{yz} orbitals, separated from d_{xy} by an energy Δt_{2g}=0.66 eV. While the planar d_{xy} charge is almost completely confined in the doped layer, about half the d_{xz} plus d_{yz} charge (0.25 electrons) spills out into STO as well, as those orbitals propagate along z. However this charge fades out rapidly while moving away from the doped plane, and substantially vanishes inside STO. Thus, at large doping our results confirm the presence of a 2DEG confined within a few STO layers, with electronic properties qualitatively similar to those found in STO/LAO[1].

Being induced by Nb electronegativity, the confinement of d_{xz}, d_{yz} charge progressively dies out as doping decreases. Indeed, at 50% doping the d_{xz} and d_{yz} DOS are almost evenly distributed through STO, although with some remnant accumulation near the doped layer. The d_{xy} charge, on the other hand, still fully belongs to the 50%-doped layer. At 25% doping (close to experimental 20%) the d_{xz} and d_{yz} charge is homogeneously spread throughout the SL with no residual accumulation near Nb layer, while the d_{xy} charge is still 2D.

The doping-controlled dimensional crossover involving the three lowest bands of the SL is even more explicit in the band structure (Fig.4): at low doping the d_{xz}, d_{yz} bands are bulk-like, but as doping increases the lowest one progressively flattens out, with a gap opening to the higher bulk-like bands. The effective mass of the lowest band $m^*_{xz,[001]}$=$m^*_{yz,[001]}$ increases from 0.39 to 0.83 to 3.85 (in electron mass units) for 25%, 50%, and 100% doping (the same mass is 0.32 in bulk $SrTi_{0.75}Nb_{0.25}O_3$). On the other hand, the lowest d_{xy} band is fully confined at any doping, with $m^*_{xy,[001]}\simeq$1000 compared to 5.45 in $SrTi_{0.75}Nb_{0.25}O_3$. A zoom near ϵ_F (Fig.4 bottom) shows that the SL spectrum is actually gapped along k_z; a non-vanishing conductivity at room T is still expected, however, because of the high DOS near ϵ_F.

Our results thus far describe this SL as a double-channel conduction system, with a portion of charge of d_{xy} orbital character fully confined in 2D at any doping concentration, and a fraction of d_{xz}, d_{yz} charge which may be 2D or 3D in nature depending on the doping concentration. As described in the following, these two channels will contribute differently to in-plane thermopower.

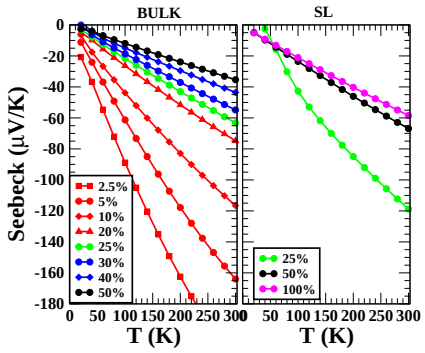

FIG. 5: Bloch-Boltzmann-calculated planar Seebeck S vs T for STO bulk (left) and the STO_9/Nb-STO_1 SL (right panel) at various Nb-doping concentrations. For bulk, calculations are actually done at 25% doping, where data at other dopings are calculated in a rigid-band approach, which is acceptable in the bulk.

B. Thermopower

We use the calculated band energies as input for the Bloch-Boltzmann transport theory[22], and calculate (Fig.5) the in-plane components of Seebeck coefficient (S) as a function of temperature for the Nb-doped STO bulk and the 10-layer SL at varying Nb doping concentration (these calculations adopt an energy-dependent modeling of relaxation time discussed in detail in the Supplementary). At equal nominal donor doping and T=300 K, the calculated Seebeck for the SL (S_{sl}) is about a factor 2 larger than in bulk (S_{bulk}), in qualitative agreement with the experiment[9,12]. Specifically, our $|S_{bulk}|$=60 μV/K at 25% doping is close to 62 μV/K measured[12] at 20%; however, our $|S_{sl}|$=120 μV/K at 25% is half the experimental 240 μV/K[12] at 20% doping. The discrepancy may be due to defects or stoichiometry fluctuations which may reduce, with respect to nominal doping, the effective mobile charge contributing to transport (similarly to what happens in STO/LAO[1]). In fact, our S_{sl} (see Fig.7) matches the experimental value at ∼8% doping (see Fig.7), corresponding to a density 1.3×10^{20}cm^{-3} not too far from value 2.2×10^{20}cm^{-3} reported in Ref.[12].

We now investigate the reason for the thermopower enhancement. In Fig.6 we show the calculated DOS (n(ϵ), upper panels), in-plane logarithmic electrical conductivity (ln$\sigma(\epsilon)$, determined to within an additive ln(F(T)), middle panels), and Seebeck (lower panels) as a function of carrier energy at T=300 K for the SL at 25% and 50% doping, and for bulk $SrTi_{0.75}Nb_{0.25}O_3$.

These results can be analyzed with the help of the Cutler-Mott formula[23]

$$S = \frac{\pi^2 k_B^2 T}{3e} \frac{\partial(\ln \sigma)}{\partial \epsilon}|_{\epsilon_F} \simeq \frac{\pi^2 k_B^2 T}{3e} \frac{1}{n} \frac{\partial n}{\partial \epsilon}|_{\epsilon_F}, \qquad (2)$$

where $\sigma(\epsilon)$=$en(\epsilon)\mu(\epsilon)K_BT$, and the mobility $\mu(\epsilon)$ is assumed energy-independent in the last term of Eq.2. The latter is consistent with our BBT results: indeed the $\sigma(\epsilon)$

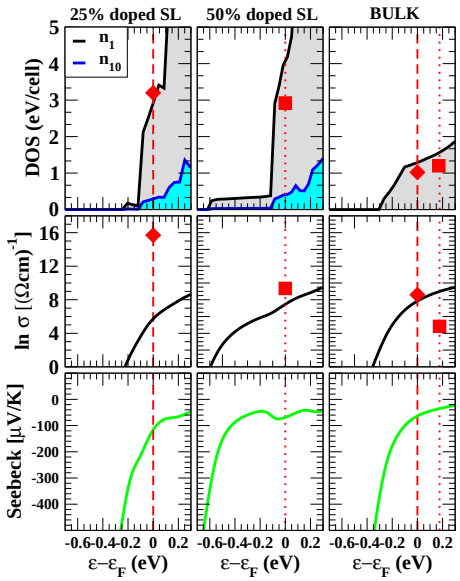

FIG. 6: Top: total DOS for the 25% and 50% Nb-doped STO_9/Nb-STO_1 SL and for the 25%-doped bulk. For the former, two different DOS are shown: n_1, normalized on a one-layer volume, and n_{10} normalized on the whole SL volume. Dashed lines: Fermi energies. Red diamond and square symbols indicate values (in eV^{-1}) of $\partial(\ln n)/\partial\epsilon|_{\epsilon_F}$ at 25% and 50% doping, respectively. Center: planar logarithmic conductivity (σ) at T=300 K. Red diamonds and squares indicate values (in eV^{-1}) of $\partial(\ln\sigma)/\partial\epsilon|_{\epsilon_F}$ at 25% and 50% doping. Bottom: planar Seebeck at T=300 K for the same systems.

logarithmic derivative (squared and diamod dots in fig.6) in the SL is about twice that in bulk, and hence so is S. Eq.2 helps further in explaining the difference between S_{bulk} and S_{sl}. If the SL charge were entirely confined in the doped layer, the relevant DOS for the SL would be n_1, normalized to the volume of a single layer (see Fig.6, top). We see that its slope increases markedly compared to the bulk DOS, indicating a genuine increase of charge localization. However, we have previously demonstrated that the charge spreads through the whole SL at any doping, thus n_{10} (normalized to the whole 10-layer SL volume) is a more appropriate choice for the SL. Since at ϵ_F the slope of n_{10} and the bulk DOS at same Nb doping are similar, we conclude that the factor-2 increase in $\partial(\ln n)/\partial\epsilon|_{\epsilon_F}$ must be due to a DOS decrease (i.e. charge dilution through the SL) rather than to a slope increase (i.e. mass enhancement).

C. Multiband modeling

Direct ab-initio calculations for generic doping values may require a workload easily exceeding the current possibilities of today computing equipments. To generalize our analysis to doping levels not accessible by direct first-principles calculations, we have used a 3-dimensional effective mass modeling[18] including all the t_{2g} conduc-

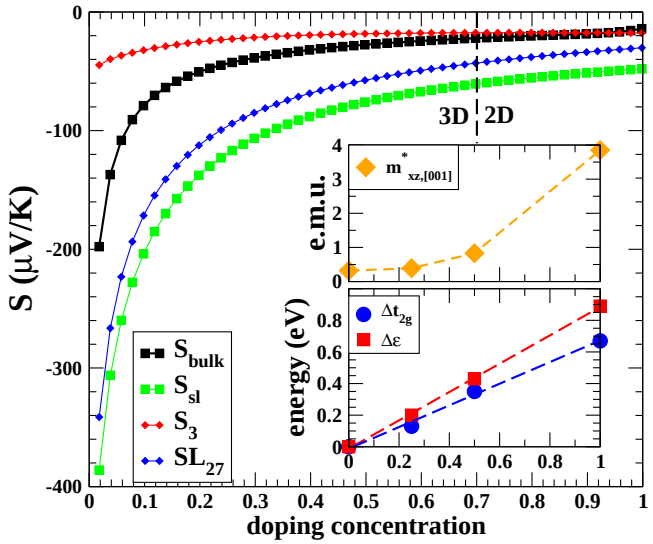

FIG. 7: Left: Thermopower as a function of Nb-doping concentration calculated using the multiband effective-mass model with doping-dependent band parameters, for STO bulk (black) and the STO_9/Nb-STO_1 SL (green line) at T=300 K. For the latter, contributions from the 3 lowest t_{2g} bands (red) and the remaining 27 t_{2g} bands (blue line) are also shown. The vertical dashed line separates regions of 3D (low-doping) and 2D (high-doping) carrier regime (see text). Inset: model parameters interpolation as a function of doping (see text).

tion bands of the full calculation (30 bands for the 10-layer SL). The inaccuracy of the rigid band approximation is circumvented using a doping-dependent band parametrization extrapolated from the VPSIC calculation for three key quantities (see Fig.7, inset): the t_{2g} energy splitting (Δt_{2g}), the energy difference between the lowest d_{xy} band and the bulk-like STO conduction band manifold ($\Delta\epsilon$), and the effective mass of the bands involved in the dimensional crossover ($m^*_{xz,[001]}$=$m^*_{yz,[001]}$). The model is finally validated by its reproducing the Bloch-Boltzmann Seebeck at 25%, 50% and 100% doping.

In Fig.7 (left, main panel) we compare S_{bulk} and S_{sl} at T=300 K vs Nb concentration. S_{sl} is further broken down into contributions from the three lowest bands (S_3) and all the other 27 t_{2g} bands (S_{27}) included in the model:

$$S_{sl} = S_3 + S_{27} = \sum_{i=1,3} \frac{\sigma_i S_i}{\sigma} + \sum_{i=4,30} \frac{\sigma_i S_i}{\sigma} \qquad (3)$$

where σ_i and S_i are conductivity and thermopower of the i^{th} band. As doping decrease we see a progressive increase in S_{sl} over S_{bulk}, as a consequence of the enhanced $|S_{27}|$ contribution. This is easily understood recalling that $|S|$ is inversely related to ϵ_F: at low doping the SL charge can be progressively diluted through a large number of bands, in turn lowering ϵ_F with respect to the bulk. At zero doping $\Delta\epsilon \sim 0$, $\Delta t_{2g} \sim 0$, and the full dilution limit S_{27}=0.9 S_{sl} is reached. On the other hand, $|S_3|$ is always smaller than $|S_{27}|$ and changes barely with doping, despite the fact that only the two lowest d_{xz}, d_{yz} bands are affected by confinement. Indeed, while the 2D confinement (i.e. the increase of $m^*_{xz,[001]}$) in itself lowers ϵ_F, the increment of doping stabilizes the three lowest bands (i.e. enhances $\Delta\epsilon$), thus causing a flow of additional charge from the higher-energy bands and effectively rising ϵ_F; the net effect is that S_3 remains nearly constant with doping, and progressively approaches S_{bulk} as Nb doping increases. Above 70% doping, $S_3 \sim S_{bulk}$ because the charge collapses into the three lowest bands (at T=0), which are now well separated from the STO band manifold. A doping of 70% is thus the estimated threshold between 3D and 2D behavior. Nevertheless, the thermal occupancy of the higher bands at T=300 K is sufficient to furnish a sizeable S_{27} contribution to the total S_{sl}, still visibly larger than S_{bulk}.

These results thus indicates that the difference between S_{bulk} and S_{sl} is mainly determined by the charge dilution through the SL, rather than by the confinement-induced charge localization. This has a simple rationale: for a single-band system, enhancing the effective mass is tantamount to reducing ϵ_F, in turn increasing the thermopower; but for a multi-band system a very tight 2D confinement may actually cause ϵ_F to rise, and be detrimental for thermopower compared to a milder confinement allowing 2DEG dilution over a larger thickness.

The effect of charge dilution on S can be easily seen in a very simple case: if a charge n_{3D} initially localized in a single band filled up to E_F is redistributed in a number of N identical bands filled up to E_F', all with the same mobility μ, charge $n_i = n_{3D}/N$, conductivity $\sigma_i = e\, n_i\, \mu$, and seebeck S_i=S(E_F'), then the conductivity of the diluted system ($\sigma = \sum_i \sigma_i = N\sigma_i$) remains unchanged of course, while the Seebeck of the diluted system:

$$S = \sum_{i=1,N} \frac{\sigma_i S_i}{\sigma} = S_i(E'_F) \qquad (4)$$

must be larger in amplitude than S(E_F) as long as E_F' is lower than E_F. That is, a pure charge dilution in a multitude of degenerate bands increase the Seebeck and leave conductivity unchanged. Of course, this is not necessarely true if we a) abandon the effective mass modeling and include the actual shape of $n_{3D}(\epsilon)$; b) include the actual dependence of μ (and then τ) on E_F. However, it is unquestionable that in general, weak 2D confinement is more favourable than tight 2D confinement to obtain large Seebeck values.

Finally, in Fig.8 we replicate the result for different values of λ, to give evidence that the fundamental conclusion of this analysis is unaffected by the choice of this parameter. Indeed, we clearly see that while absolute values of total and band-decomposed Seebeck do depend on λ, the contribution of the 27 minority-occupied bands is always dominating over the 3 bands of the doped layer. Thus, we can conclude saying that independently on the

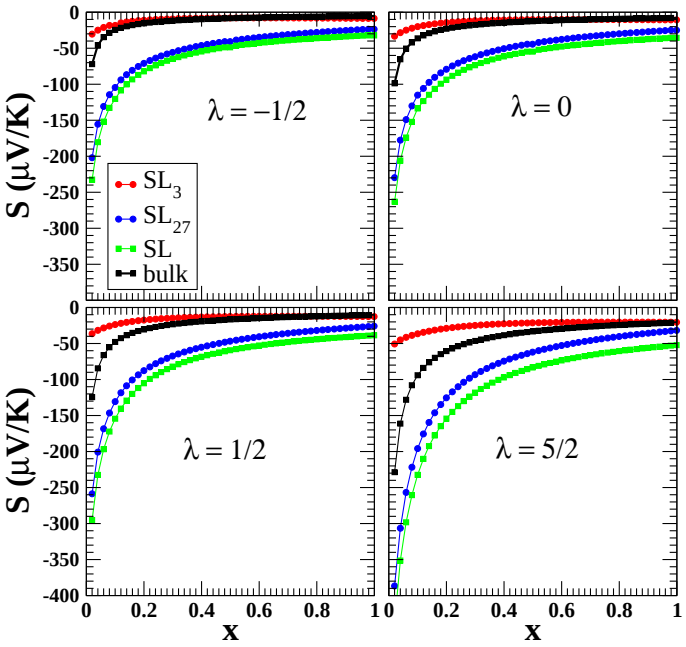

FIG. 8: Left: Thermopower as a function of Nb-doping concentration calculated using the multiband effective-mass model with doping-dependent band parameters, for STO bulk (black) and the STO_9/Nb-STO_1 SL (green line) at T=300 K. For the latter, contributions from the 3 lowest t_{2g} bands (red) and the remaining 27 t_{2g} bands (blue line) are also shown. Results of different panels only differ for the value of the power parameter λ in Eq.1.

scattering regime, charge dilution is always effective in producing an important burst in thermopower.

V. CONCLUSIONS

In conclusion, we have described from a theoretical viewpoint the characteristics of the electron gas present in 10-layer Nb-doped oxide superlattices. We showed that the electronic properties (effective mass and spatial extension) of the mobile charge in the SL can be effectively tuned by the diagnostic choice of the doping concentration: above the estimated threshold of 70% doping a dimensional crossover take place, and a fully confined 2DEG appears. Below this threshold, electron charge accumulates near the doped layer, but a consistent fraction of it (progressively increasing with the lowering of doping concentration) spreads thorugh the whole SL, so that a complete 2D confinement is not acheved. We remark that very high Nb-doping concentrations in STO are experimentally achievable, and apparently keen to the reach of high electron mobility[11].

In agreement with the experiments[9,10], we find the thermopower of the SL remarkably larger than the thermopower of the bulk at equivalent doping concentration. Such an increase of thermopower is found to be consequence of the delocalization of carriers into a multitude of barely occupied bands. This conclusion can be understood considering that, according to the Boltzmann theory, the dominant factor in expanding the Seebeck amplitude is primarily the lowering of the Fermi energy which obviously follows from the dilution.

As a general rule, our analysis shows that in a multiband system, a weak 2D confinement favors large thermopower more than a strong confinement which tightly traps all the charge in one or a few doped layers.

Acknowledgments

Work supported in part by projects EU FP7 *OxIDes* (grant n.228989), MIUR-PRIN 2010 *Oxide*, IIT-Seed *NEWDFESCM*, IIT-SEED POLYPHEMO and "platform computation" of IIT, 5 MiSE-CNR, Fondazione Banco di Sardegna 2011. MJV acknowledges a visiting professor grant at Cagliari University, the Belgian ARC project TheMoTherm, and a "Crédit d'impulsion" grant from University of Liège. Calculations performed at CASPUR Rome and Cybersar Cagliari.

[1] A. Ohtomo and H. Y. Hwang, Nature **427**, 423 (2004); S. Thiel *et al.*, Science **313**, 1942 (2006); M. Huijben *et al.*, Nature Mater. **5**, 556 (2006); N. Reyren *et al.*, Science **317**, 1196 (2007); I. Pallecchi *et al.*, Phys. Rev. B **81**, 085414 (2010)).
[2] R. Venkatasubramanian, E. Siivola, T. Colpitts, and B. O'Quinn, Nature **413**, 597 (2001).
[3] T. C. Harman, P. J. Taylor, M. P. Walsh, and B. E. LaForge, Science **297**, 2229 (2002).
[4] A. Majumdar, Science, **303**, 777 (2004).
[5] M. S. Dresselhaus, *et al.* Adv. Mater. **19**, 1 (2007).
[6] C. B. Vining, Nature **423**, 391 (2007).
[7] K. Biswas, *et al.*, Nature **489**, 414 (2012).
[8] L. E. Bell, Science, **321**, 1457 (2008).
[9] H. Ohta *et al.*, Nature Materials **6**, 129 (2007).
[10] B. Jalan and S. Stemmer, Appl. Phys. Lett. **97**, 042106 (2010).
[11] T. Tomio, *et al.*, J. Appl. Phys., **76**, 5886 (1994).
[12] Y. Mune *et al.*, Appl. Phys. Lett. **91**, 192105 (2007).
[13] H. Ohta *et al.*, Thin Solid Films **516**, 5916 (2008).
[14] L. D. Hicks and M. S. Dresselhaus, Phys. Rev. B **47**, 12727 (1993); L. D. Hicks *et al.*, Phys. Rev. B **53**, 10493 (1996).
[15] J. O. Sofo and G. D. Mahan, Appl. Phys. Lett. **65**, 2690 (1994).
[16] D. A. Broido and T. L. Reinecke, Phys. Rev. B **51**, 13797 (1995); Appl. Phys. Lett. **67**, 1170 (1995).
[17] H. Usui *et al.*, Phys. Rev. B **81**, 205121 (2011).
[18] A. Filippetti, *et al.*, Phys. Rev. B **86** 195301 (2012).
[19] A. Filippetti *et al.*, Phys. Rev. B **84**, 195127 (2011); A. Filippetti and N. A. Spaldin, Phys. Rev. B **67**, 125109

(2003); A. Filippetti and V. Fiorentini, Eur. Phys. J. B **71**, 139 (2009).
[20] P. Delugas *et al.*, Phys. Rev. Lett. **106**, 166807 (2011).
[21] D. Puggioni, *et al.*, Phys. Rev. B **86** 195132 (2012).
[22] G. Madsen and D. Singh, Computer Physics Communications **175**, 67 (2006).
[23] M. Cutler and N. F. Mott, Phys. Rev. **181**, 1336 (1969).
[24] T. Okuda *et al.*, Phys. Rev. B **63**, 113104 (2001).
[25] K. Durczewski and M. Ausloos, Phys. Rev. B **61**, 5303 (2000).
[26] S. Ohta *et al.*, J. of Applied Phys. **97**, 034106 (2005).